Exploration of Drug Science

Open Exploration

Open Access Original Article

Chitosan-based nanoparticles fabricated by ionotropic gelation using two types of polyphosphates: characterization and in-vitro release modeling of curcumin

Ilya Eydelman[1,2], Doron Yariv[2], Shimon Ben-Shabat[1*], Amnon C. Sintov[2,3*]

[1]Department of Clinical Biochemistry and Pharmacology, Ben-Gurion University of the Negev, Be'er Sheva 8410501, Israel
[2]Laboratory for Biopharmaceutics, E.D. Bergmann Campus, Ben-Gurion University of the Negev, Be'er Sheva 8410501, Israel
[3]Department of Biomedical Engineering, Ben-Gurion University of the Negev, Be'er Sheva 8410501, Israel

***Correspondence:** Shimon Ben-Shabat, Department of Clinical Biochemistry and Pharmacology, Ben-Gurion University of the Negev, Be'er Sheva 8410501, Israel. sbs@bgu.ac.il; Amnon C. Sintov, Department of Biomedical Engineering, Ben-Gurion University of the Negev, Be'er Sheva 8410501, Israel. asintov@bgu.ac.il

Academic Editor: Xiqun Jiang, Nanjing University, China
Received: January 8, 2026 **Accepted:** February 26, 2026 **Published:** April 15, 2026

Cite this article: Eydelman I, Yariv D, Ben-Shabat S, Sintov AC. Chitosan-based nanoparticles fabricated by ionotropic gelation using two types of polyphosphates: characterization and in-vitro release modeling of curcumin. Explor Drug Sci. 2026;4:1008157. https://doi.org/10.37349/eds.2026.1008157

Abstract

Aim: Chitosan (CHS)-based nanoparticulate systems have gained much interest due to their high drug loading capacity and the simplicity of their fabrication. The physical properties of two types of curcumin-loaded CHS nanoparticles (CHS-NPs) were determined and compared. A new in-vitro release method was developed based on mathematical modeling in which the drug is first released from the NP into the surrounding medium and subsequently diffuses through the membrane.

Methods: Curcumin-loaded CHS-NPs were fabricated by ionotropic gelation using sodium tripolyphosphate (TPP) and sodium hexametaphosphate (SHMP) crosslinking, and characterized by NP tracking analysis, loading capacity, zeta potential, Fourier transform infrared spectroscopy (FTIR), and in-vitro release rates.

Results: The data showed that compared to SHMP crosslinked CHS-NPs, TPP crosslinking demonstrated a decrease in entrapment efficiency at a relatively high concentration of the agent, probably by narrowing the space between the polymeric chains. As indicated by zeta potential measurements, TPP crosslinking at all levels was more uniformly distributed inside the NPs, whereas the higher molecular weight SHMP at a low concentration creates NPs mostly by binding onto the surface. It was found that the release rates of curcumin from CHS-NPs crosslinked by SHMP at higher concentrations were about twice as high as the release rates of curcumin from TPP-crosslinked CHS-NPs, accompanied by notable lag times.

Conclusions: This significant increase in the release rates of curcumin from SHMP-crosslinked CHS-NPs is explained by the large spatial structure of this crosslinker compared to the small TPP molecules. This study advances the literature on drug diffusion by making it possible to accurately determine its release from nanoparticulate systems.

Keywords

chitosan nanoparticles, curcumin, tripolyphosphate, sodium hexametaphosphate, in-vitro release

Introduction

Nanoparticles (NPs) based on natural polysaccharides have been intensely studied due to their biocompatibility, biodegradability, non-immunogenicity, and environmentally benign nature. Besides its general properties as a natural polysaccharide, chitosan (CHS), a linear cationic polysaccharide, displays many attractive properties. To name a few, it has been shown to be mucoadhesive [1–3] and is known to have wound healing activities [4–6]. CHS has gained a widespread interest in the last couple of decades as an adequate nanoparticulate carrier [4, 7–9], as its NPs have demonstrated enhanced delivery and biodistribution of drugs by opening tight junctions [10, 11]. In addition, CHS-NPs have shown increased cellular uptake by cationic ligands with protein domains on the cell surface [12].

There are various methods that have been utilized for manufacturing CHS-NPs. They are basically classified into 'coacervation' and 'emulsification' methods [13, 14]. Coacervation methods include ionotropic gelation, polyelectrolyte complexation, and desolvation [15], while emulsification methods include emulsion droplet coalescence, emulsion solvent diffusion, and reverse micellization. CHS-NPs loaded with various drugs were demonstrated to enhance drug activity and improve cellular uptake of therapeutics [16–18]. The most popular and commonly preferred method of CHS-NP preparation is the coacervation method based on ionotropic gelation and ionotropic gelation/polyelectrolyte complexation [19], mainly due to its simplicity and because it does not involve addition of an organic solvent. Ionotropic gelation of CHS was first described by Calvo et al. [20], who used sodium tripolyphosphate (TPP) as the polyanionic cross-linker. TPP has frequently been used as the negatively charged polyanion, however, sodium hexametaphosphate (SHMP) has also been reported, although less frequently, as ionotropic crosslinker agent for the preparation of CHS-NPs [21–23]. In the present paper, we used curcumin (CUR) as the model agent. CUR is a natural polyphenolic compound possessing many beneficial properties, including anticancer, antioxidant, antimicrobial, anti-inflammatory, and neuroprotective activities [24–29]. CHS-NPs loaded with CUR were prepared using various methods [30–33]. CUR-containing CHS-NPs (combined with other antioxidants) have been prepared using SHMP [34], but the overall literature on this nano-system is lacking. A comparison of CUR-containing CHS-NPs prepared using the two different commonly-used cross-linkers has not previously been studied and reported. The aim of the current study was to explore the properties of CUR-loaded CHS-NPs fabricated using SHMP crosslinker and to compare them with particles prepared by the more commonly used TPP crosslinker. It was hypothesized that due to the structural differences between the two crosslinking molecules, TPP and SHMP, NPs with different characteristics would be formed. Hence, the physical properties of CUR-loaded CHS-NPs, which were prepared by TPP and SHMP, were analyzed, determined, and compared. Furthermore, the release rates of CUR from the various NPs were determined using the Franz cell system as previously published by our group [35, 36], providing an improved precision.

Materials and methods

Materials

CHS [low molecular weight: 50–190 kDa, degree of deacetylation ≥ 75%, viscosity: 20–300 cP, 1% (w/w) in 1% acetic acid], SHMP, Tween 80 and tablets for phosphate buffered saline (PBS) preparation were obtained from Sigma Aldrich (Sigma-Aldrich Israel Ltd., Rehovot, Israel). TPP from Santa Cruz Biotechnology Inc. (Dallas, TX, USA). CUR was obtained from Glentham Life Sciences Ltd. (Corsham, United Kingdom). Acetic acid glacial was purchased from Merck (Darmstadt, Germany). Ethyl alcohol AR was purchased from BioLab Ltd. (Jerusalem, Israel). Methanol and high-performance liquid chromatography (HPLC) grade solvents were obtained from J.T. Baker (Mallinckrodt Baker, Inc., Phillipsburg, NJ).

Preparation of CHS-NPs

CUR-loaded CHS-NPs were prepared using the ionic gelation method [37–41]. CHS (12 mg) was dissolved by consecutive addition of acetic acid glacial (150 µL) and double-distilled water (DDW) (40 mL). This mixture was stirred using a magnetic bar at 700 rpm for 10 min, and the pH was measured (pH = 3.0–3.2). NaOH 1 N solution was then added at 0.2 mL/min by a syringe pump (NE-300, New Era Pump Systems, Farmingdale, NY, USA) with continuous pH monitoring until pH = 5. Separately, CUR was dissolved in ethanol (5 mg/2.5 mL) and sonicated for 480 s. Tween 80 (90 µL volume) was added, and the mixture was vortexed. Even though CUR had been dissolved in ethanol [42, 43], Tween 80 was added to avoid CUR precipitation prior to the formation of NPs in the aqueous environment. The use of Tween 80 was previously described in the context of ionic gelation method [44]. Various TPP or SHMP quantities (Table 1) were dissolved in DDW and added to the CUR solution and the total volume was made up to 4 mL for all combined components. This mixture dripped into the CHS solution using a syringe pump at 0.1 mL/min for TPP or 0.05 mL/min for SHMP with under stirring (500 rpm) (Figure 1). The lower dripping rate of SHMP was required since larger particles were formed at higher rates. The mixture of the combined solutions was further stirred for 1 h at 400 rpm. This step was performed at a slightly slower stirring rate to allow complete cross-linking and particle stabilization, while minimizing aggregation.

Table 1. A summary of the prepared CHS nanoparticulate formulations.

Formulation	Cross-linker	CUR added (mg CUR/mg CHS)	Polyanion added (mg/mg CHS)	Polyanion level (mmol/mg CHS)
CHS-T1	TPP (sodium salt)	0.417	0.025	0.068
CHS-T2			0.050	0.136
CHS-T3			0.083	0.226
CHS-T4			0.125	0.340
CHS-S1	SHMP	0.417	0.042	0.068
CHS-S2			0.083	0.136
CHS-S3			0.139	0.226
CHS-S4			0.208	0.340

CHS: chitosan; CUR: curcumin; SHMP: sodium hexametaphosphate; TPP: sodium tripolyphosphate.

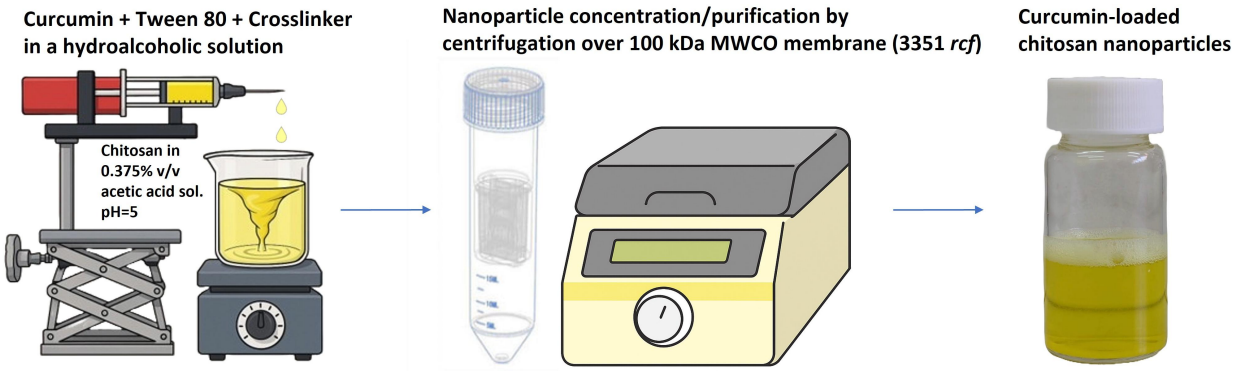

Figure 1. Schematic representation of batch process manufacturing of curcumin-loaded chitosan nanoparticles.

Determination of CUR content in NPs

The NPs dispersions were filtered using ultra centrifugal filter with 100 kDa MWCO membrane (Amicon Ultra from Merck Millipore Ltd., Cork, Ireland) at 3,351 *rcf*, 30 min, 25°C (Figure 1). The liquid that was obtained after filtration was collected, diluted ×10 with methanol and analyzed by HPLC. This liquid that crossed the membrane represented the free unloaded CUR molecules. The samples were injected into a HPLC system (1260 Infinity II, Agilent Technologies Inc., Santa Clara, CA), equipped with a prepacked column (BetaSil C18, 5 µm, 250 mm × 4.6 mm, Thermo Fisher Scientific). The samples were chromatographed using a mobile phase consisting of acetonitrile/acetic acid 0.2% solution (75:25) at a flow rate of 1 mL/min. Calibration curves, peak areas measured at 425 nm for CUR versus drug concentration,

were constructed by running standard drug solutions in methanol for each series of chromatographed samples. The limit of detection (LOD) was 0.1 μg/mL and the limit of quantification (LOQ) was 0.25 μg/mL. The mass of CUR in the NPs was calculated by subtracting the obtained data of unloaded CUR from the total mass of CUR added in the preparation process.

Encapsulation (or entrapment) efficiency percentage (EE%) was calculated according to the following equation:

$$EE\% = \frac{Total\ CUR\ (added) - Free\ CUR\ (analyzed)}{Total\ CUR\ added\ in\ formulation} \times 100 \quad (1)$$

NP tracking analysis (NTA)

Measurements were performed using a NanoSight NS300 instrument (Malvern Instruments Ltd., Worcestershire, UK), equipped with a 642 nm red laser module and 450 nm long-pass filter, and a camera operating at 25 frames per second, capturing a video file of the particles moving at a constant flow rate from a syringe on a syringe pump. The software for capturing and analyzing the data (NTA 3.4) calculated the hydrodynamic diameters of the particles by using the Stokes-Einstein equation. Depending on the NP concentration, each measurement provided data about size distribution (in diameter) for approximately 5,000–15,000 particles.

Zeta (ζ) potential

The samples were diluted to appropriate concentration using DDW and transferred to U-tube cuvette (DTS1060C, Malvern). Measurement was performed using Zeta sizer (ZN-NanoSizer, Malvern, UK). The particles were measured in automatic mode at 25°C.

Transmission electron microscopy (TEM)

TEM images were recorded with Talos F200C (Thermo Fisher Scientific) transmission electron microscope operating at 200 kV. Samples of CHS-NPs dispersions were deposited on a copper grid, coated with Formvar and carbon (Electron Microscopy Sciences, Fort Washington, PA, USA) and left to stand for 1 min, then the excess liquid was adsorbed using filter paper. The images were taken with Ceta 16M CMOS camera.

Fourier transform infrared spectroscopy (FTIR)

CHS-NPs and their individual components (CHS, CUR, TPP and SHMP) were analyzed using Nicolett 6700 FTIR spectrometer (Thermo Fisher Scientific). Samples of CHS-NPs were lyophilized for 24 h prior to examination. Infrared (IR) spectra of the various samples were recorded over a range of 4,000–500 cm^{-1}.

In-vitro release study

Permeation of CUR solution

The permeability of CUR through a hydrophobic polytetrafluoroethylene (PTFE) membrane (Starlab Scientific, 0.1 μm pore size, 25 mm diameter) was measured using a Franz diffusion cell system (Permegear, Inc., Bethlehem, PA, USA). The diffusion area was 1.767 cm^2 (15 mm diameter orifice), and the receiver compartment volumes were 12 mL. The solution in the receiver compartment ("receiver solution") consisted of PBS (0.01 M, pH 7.4) containing 10% (v/v) Tween 80, 0.01% (w/v) butylated hydroxytoluene (BHT), and 5% (v/v) methanol. CUR was dissolved in dimethyl sulfoxide (DMSO) (11 mg/mL), further diluted with the receiver solution and aliquoted to a volume of 0.58 mL containing 120 μg of CUR (DMSO final concentration = 1.9%). The CUR solution was placed in the donor compartment. The solution on the receiver side was stirred by externally driven, Teflon-coated magnetic bars and maintained at 37°C. At predetermined time points, samples of 1 mL from the receiver solution were withdrawn and kept for HPLC analysis. After every sampling, 1 mL of fresh solution was replenished to the volume. Each set of experiments was performed in triplicate (n = 3). A perfect sink condition in the receiver compartment was maintained throughout the permeation and the release experiments by using a relatively large volume of a receiver solution containing alcohol and a surfactant as described above. These conditions and the constant dilution ensured CUR solubility far in excess of the maximum theoretical receiver concentration of CUR.

CUR release from NPs and permeation through the membrane

Aliquots (0.5–0.6 mL) of CHS-NP dispersions were placed in the donor compartment. The two compartments (donor and receiver) were separated by a membrane permeable to CUR but impermeable to the NPs (PTFE membrane, 0.1 µm pore size, 25 mm diameter). The NPs were placed in the donor compartment, and the released CUR permeated through the membrane to the receiver compartment. Various CHS-NP formulations, each containing 120 µg of CUR in 0.5–0.6 mL volumes, were placed in the donor compartment. The experiments with the NPs were performed as mentioned above, except they were performed for 66 h instead of 48 h. Each set of experiments was performed in triplicate (n = 3).

Calculation of CUR permeation through the membrane

Because of the sampling of large volumes from the receiver solution (and their replacement with equal volumes of buffer), the receiver solution was constantly being diluted. Taking this process into account, the cumulative drug that permeated out into the receiver [$Q_{out}(t_n)$] at the end of the n^{th} sampling time ($n \geq 0$) was calculated according to the following equation:

$$Q_{out}(t_0) = C_{out}(t_0) = 0; \quad t_0^- = t_0 = 0 \tag{2}$$

$$Q_{out}(t) = V_r\, C_{out}(t_n^-) + \sum_{i=0}^{n-1} V_s\, C_{out}(t_n^-) \quad n \geq 1 \tag{3}$$

$$C_{out}(t_n) = \left[C_{out}(t_n^-) \cdot (V_r - V_s)\right] / V_r \tag{4}$$

Where $C_{out}(t_n)$ is the drug concentration in the receiver at sampling time t_n, expressed by a running number $(t = 1,\ 2,\ 3 \ldots t_n)$. V_r and V_s are the constant volumes of the receiver and the sample solutions, respectively. Data was expressed as the cumulative permeated drug per unit of membrane surface area, $Q_{out}(t_n) / S$ (S = 1.767 cm^2).

Calculation of the membrane permeability coefficient (P)

The release of CUR from the NPs was performed in a Franz diffusion cell system using a synthetic membrane. The permeability coefficient of the membrane was calculated by linear regression of the experimental data of cumulative permeation of the free drug in plain solutions (P) as previously described by Sintov [36]. Drug transport across the membrane is governed by the integral form of Fick's law:

$$\frac{dQ_{out}}{dt} = \frac{D \cdot S \cdot K \cdot (C_{in} - C_{out})}{h} \tag{5}$$

$$\frac{dQ_{out}}{dt} = P \cdot S \cdot (C_{in} - C_{out}); \quad P = \frac{D \cdot K}{h} \quad t_0 < t \quad Q_{out}(0) = 0 \tag{6}$$

where, dQ_{out} / dt is the permeation flux across the dialysis membrane, D is the drug diffusion coefficient through the membrane, S is the membrane surface area, K is the membrane partition coefficient of the drug, and h is the membrane thickness. The expression $K(C_{in} - C_{out})$ is proportional to the developing concentration gradient across the membrane.

$$C_{in} = \frac{(Q_{tot} - Q_{out})}{V_d} \tag{7}$$

$$C_{out} = \frac{Q_{out}}{V_r} \tag{8}$$

where, Q_{tot} is the initial amount of the drug in the donor compartment, V_d is the volume of the solution (or NP dispersion) in the donor compartment, and V_r is the volume of the solution in the receiver compartment. Therefore, Equation 6 can be transformed into:

$$\frac{dQ_{out}}{dt} = P \cdot S \cdot \left(\frac{Q_{tot} - Q_{out}}{V_d} - \frac{Q_{out}}{V_r}\right) \tag{9}$$

and after simplifying:

$$\frac{dQ_{out}}{dt} + P \cdot S \cdot \left(\frac{1}{V_d} + \frac{1}{V_r}\right) \cdot Q_{out} = P \cdot S \cdot \left(\frac{Q_{tot}}{V_d}\right) \tag{10}$$

Denoting:

$$\alpha = P \cdot S \cdot \left(\frac{1}{V_d} + \frac{1}{V_r}\right) \tag{11}$$

$$\beta = P \cdot S \cdot \left(\frac{Q_{tot}}{V_d}\right) \tag{12}$$

then,

$$\frac{dQ_{out}}{dt} + \alpha \cdot Q_{out} = \beta \tag{13}$$

whose solution is:

$$Q_{out}(t) = \frac{\beta}{\alpha}[1 - exp(-\alpha t)] \tag{14}$$

Noting that this leads to:

$$exp(-\alpha t) = 1 - (\alpha / \beta) Q_{out}(t) \tag{15}$$

or:

$$ln\left[1 - (\alpha / \beta) Q_{out}(t)\right] = -\alpha t \tag{16}$$

and since,

$$\alpha / \beta = \frac{V_r + V_d}{V_r \cdot Q_{tot}} \tag{17}$$

Hence:

$$ln\left[1 - \left(\frac{V_r + V_d}{V_r \cdot Q_{tot}}\right) Q_{out}(t)\right] = -P \cdot S\left(\frac{V_r + V_d}{V_d \cdot V_r}\right) t \tag{18}$$

Thus, a plot of $ln\left[1 - \left(\frac{V_r + V_d}{V_r \cdot Q_{tot}}\right) Q_{out}(t)\right] \cdot \left[\frac{-V_d \cdot V_r}{S(V_r + V_d)}\right]$ against t would yield a linear slope from which P can be derived for plain drug solutions.

Calculation of the drug release rate

The release rate of the drug from NPs can be calculated according to Gupta et al. [45]. Assuming the release of CUR from the NPs follows a zero-order process, then:

$$\frac{dQ_n}{dt} = -k_{rel} \tag{19}$$

where, Q_n is the amount of drug in the NPs at time t, and k_{rel} is the release rate constant of the drug from the NPs.

After integration:

$$Q_n = Q_n^0 - k_{rel} \cdot t \tag{20}$$

$$at\ t_0 = 0,\quad Q_n = Q_n^0 = Q_{tot} \tag{21}$$

and rearrangement:

$$Q_n^0 - Q_n = k_{rel} \cdot t \tag{22}$$

Since $\left(Q_n^0 - Q_n\right)$ is the amount of drug released from the NPs at time t, it can be substituted for $(Q_{in} + Q_{out})$ or $(C_{in}V_d + C_{out}V_r)$ that expresses the drug quantity in both the donor and the receiver compartments.

$$C_{in}V_d + C_{out}V_r = k_{rel} \cdot t \tag{23}$$

after dividing by V_d:

$$C_{in} = \frac{k_{rel}t}{V_d} - \frac{C_{out}V_r}{V_d} \tag{24}$$

At t = 0, the NPs were suspended in buffer and immediately applied into the donor compartment. For this case, an initial free drug $C_{in} = C_{in}^0$; however, C_{in}^0 is negligible considering the very low solubility of CUR, thus the initial free drug $C_{in} = C_{in}^0 = 0$:

$$C_{in} = C_{in}^0 + \frac{k_{rel}t}{V_d} - \frac{C_{out}V_r}{V_d}; \quad C_{in}^0 = 0 \tag{25}$$

Combining Equation 6 with Equation 25 gives:

$$\frac{dC_{out}}{dt} = \frac{P \cdot S \cdot (C_{in} - C_{out})}{V_r} = \frac{P \cdot S}{V_r}\left(\frac{k_{rel}t}{V_d} - \frac{C_{out}V_r}{V_d} - C_{out}\right) \tag{26}$$

Equation 26 is solved by Laplace transforms and its expression is simplified by defining a as: $a = \frac{P \cdot S(V_r + V_d)}{V_r V_d}$.

$$C_{out} = \frac{k_{rel}}{(V_r + V_d)}\left[t - \frac{1}{a}(1 - e^{-at})\right] \tag{27}$$

A plot of C_{out} versus $\frac{1}{(V_r + V_d)}\left[t - \frac{1}{a}(1 - e^{-at})\right]$ would yield a linear slope from which the drug release rate constant k_{rel} can be derived.

Statistical analysis

The statistical differences between the release data of CUR obtained from the various CHS-NP formulations were analyzed employing the two-way unweighted means analysis of variance (ANOVA) test and Student's *t*-test for multiple comparisons. The differences among groups were considered significant when p values < 0.05.

Results

NP characterization

CHS-NPs were prepared by ionotropic gelation using two polyphosphate crosslinkers, TPP and SHMP, at 0.068, 0.136, 0.226, and 0.340 mmol/mg of CHS. Table 2 summarizes the particle size, particle size distribution [polydispersity index (PDI)], particle concentration, and ζ potential as well as CUR loading and EE of the various nanoparticulate systems. The systems were prepared with four different polyanion levels, i.e., four TPP levels and four SHMP levels. Figure 2 shows the morphological shapes of representative NPs, a TPP-crosslinked CHS-NP and a SHMP-crosslinked CHS-NP. Both NPs had spherical or elliptical shapes ranging in size between 200 to 300 nm. Using NTA, the mean particle size was within the range of 226–284 nm and 264–317 nm for TPP-crosslinked NPs and SHMP-crosslinked NPs, respectively.

As shown in Table 2, CUR loading and the EE, were not dependent on the SHMP concentrations within the tested range, whereas approximately 0.3 mg/mg and 74–79% were determined for CUR loading and EE, respectively. Unlike SHMP crosslinking, CHS-NPs crosslinked by TPP at a concentration of 0.340 mmol/mg CHS demonstrated a significant decrease in CUR loading and in the calculated EE, 0.25 mg/mg and 59%, respectively.

In addition to size and loading parameters, surface charge characteristics were evaluated in order to assess the influence of crosslinker type and CUR incorporation on NP interfacial properties. The ζ potential data obtained for the various CHS-NPs (Table 2) showed the following phenomena: (a) CUR loading significantly increased the ζ potential of NPs crosslinked by TPP or SHMP at concentrations of 0.068, 0.136, and 0.226 mmol/mg polymer; (b) TPP-crosslinked NPs demonstrated a constant ζ potential (an average of 33.1 ± 1.7 mV) when CUR had been added at all crosslinker's levels tested. In the absence of CUR, a constant ζ potential existed only at crosslinker's levels of 0.068 to 0.226 mmol/mg polymer (an average of 25.6 ± 1.7 mV), while at 0.340 mmol TPP/mg CHS, the ζ potential was similar in loaded and unloaded NPs (~32

Table 2. A summary of curcumin (CUR) encapsulation (or entrapment) efficiency percentage (EE%), particle size, distribution [polydispersity index (PDI)], particle concentration, and zeta (ζ) potential of CUR-loaded chitosan nanoparticle (CHS-NP) formulations.

Formulation	Sodium tripolyphosphate (TPP)-crosslinked CHS-NPs				Sodium hexametaphosphate (SHMP)-crosslinked CHS-NPs			
	T-1	T-2	T-3	T-4	S-1	S-2	S-3	S-4
Cross-linker level (mmol/mg CHS)	0.068	0.136	0.226	0.340	0.068	0.136	0.226	0.340
CUR loading (mg/mg NPs)	0.31	0.32	0.38	0.25	0.32	0.33	0.31	0.32
EE%	74	77	91	59	78	79	74	78
Particle size (nm) (mean ± SD)	283.6 ± 3.3	284.2 ± 21.0	226.6 ± 71.6	242.4 ± 21.2	264.2 ± 4.4	311.5 ± 15.2	276.3 ± 3.0	317.1 ± 1.3
PDI	0.28	0.24	0.14	0.16	0.2	0.1	0.13	0.1
D10 (nm)	137.3	149.7	152.5	140.7	144.8	203	167	204
D50 (nm)	231.6	249.2	237.3	225.6	241.7	292.5	261.5	301.4
D90 (nm)	507.5	475	372.2	364.6	399.1	445.1	409.5	449.5
NP concentration (NPs/mL) (mean ± SD)	$2.0 \times 10^{10} \pm 1.08 \times 10^{9}$	$4.02 \times 10^{10} \pm 2.14 \times 10^{9}$	$3.11 \times 10^{10} \pm 1.91 \times 10^{9}$	$5.07 \times 10^{10} \pm 2.37 \times 10^{9}$	$2.81 \times 10^{10} \pm 2.02 \times 10^{9}$	$9.27 \times 10^{10} \pm 4.41 \times 10^{9}$	$2.05 \times 10^{11} \pm 5.67 \times 10^{9}$	$1.04 \times 10^{11} \pm 2.89 \times 10^{9}$
ζ potential (mV)-CUR-loaded NPs (mean ± SD)	34.7 ± 0.7	31.1 ± 1.7	34.4 ± 3.6	32.2 ± 3.3	24.8 ± 1.35	30.8 ± 1.7	29.6 ± 2.3	29.0 ± 0.4
ζ potential (mV)-unloaded (blank) NPs (mean ± SD)	26.8 ± 3.4	26.3 ± 5.0	23.6 ± 2.7	32.1 ± 5.2	15.6 ± 1.6	23.1 ± 3.0	25.0 ± 2.2	34.6 ± 1.9

mV); (c) SHMP-crosslinked NPs demonstrated a constant ζ potential when CUR had been added at crosslinker's levels of 0.136 mmol/mg CHS and above (an average of 29.8 ± 0.9 mV). However, at 0.068 mmol SHMP/mg CHS, ζ potential was lower than the values obtained at higher crosslinker's levels; (d) In the absence of CUR, ζ potential values of SHMP-crosslinked CHS-NPs were directly dependent on the level of the crosslinker, increasing from 15.6 ± 1.6 mV to 34.6 ± 1.9 mV at SHMP levels of 0.068 mmol/mg up to 0.340 mmol/mg, respectively.

Figure 3 shows the FTIR spectra of two TPP-crosslinked CHS-NPs (0.136 and 0.340 mmol TPP/mg polymer; CHS-T2, T4), and two SHMP-crosslinked CHS-NPs (0.136 and 0.340 mmol SHMP/mg polymer; CHS-S2, S4). As shown in the figure, the spectra of these samples are similar with all their characteristic peaks: N–H and/or O–H stretching vibrations (3,362 cm^{-1} or 3,373 cm^{-1}; wide bands), C–H stretching vibrations (2,924 cm^{-1} and 2,857 cm^{-1}), carbonyl stretching vibrations (1,653 cm^{-1}; very small peak), stretching vibrations of amide (1,570 cm^{-1}), and C–O or P–O stretching vibrations (1,099 cm^{-1}).

The FTIR spectra also indicated that TPP-crosslinked NPs, particularly the CHS-T2 sample, exhibited higher intensity of C–H, N–H, and O–H vibrations (peaks at 3,200–2,900 cm^{-1}) compared with the spectra obtained from the SHMP-crosslinked NPs.

Another spectral feature was observed at 1,570 cm^{-1}, 1,407 cm^{-1}, in which the vibrational intensity is similar for the formulations CHS-T4, CHS-S2, and CHS-S4, and significantly lower (also with a higher transmittance) for the CHS-T2 sample. Spectral data of the raw materials are presented in Figure S1.

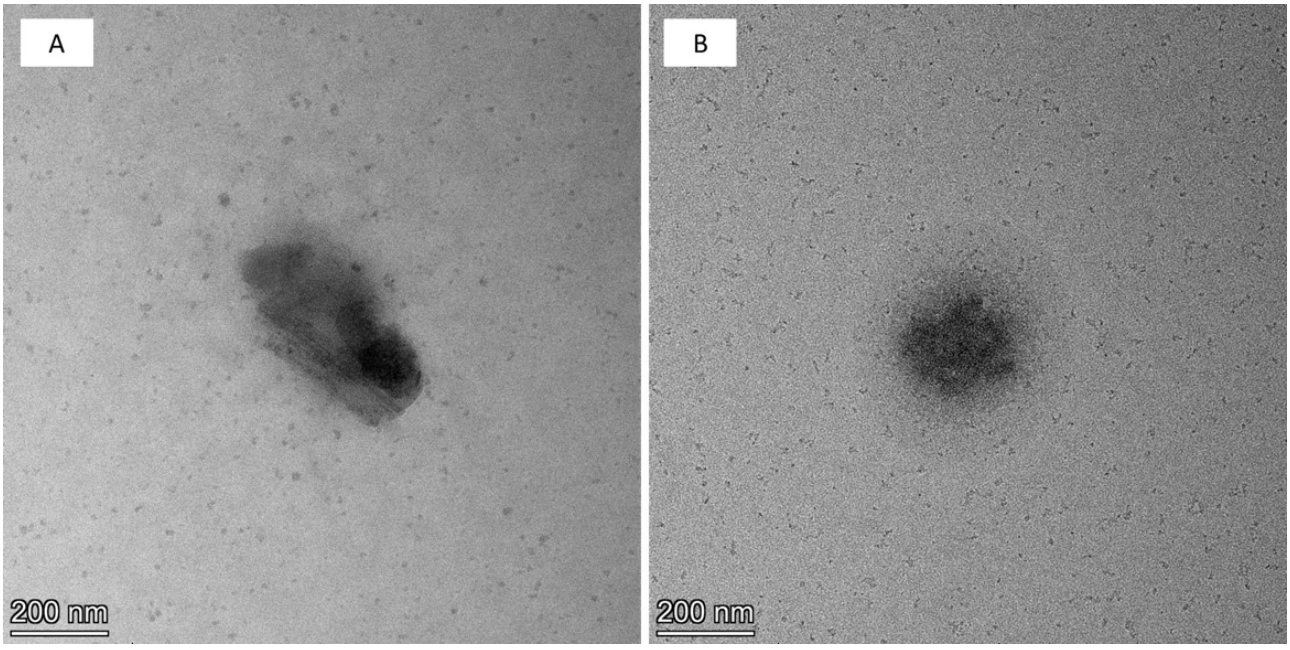

Figure 2. Transmission electron microscopy (TEM) images of chitosan nanoparticle (CHS-NP) formulations crosslinked with sodium tripolyphosphate (TPP) (A) and sodium hexametaphosphate (SHMP) (B) both at 0.340 mmol polyphosphate/mg of CHS. Images taken at ×45,000 magnification.

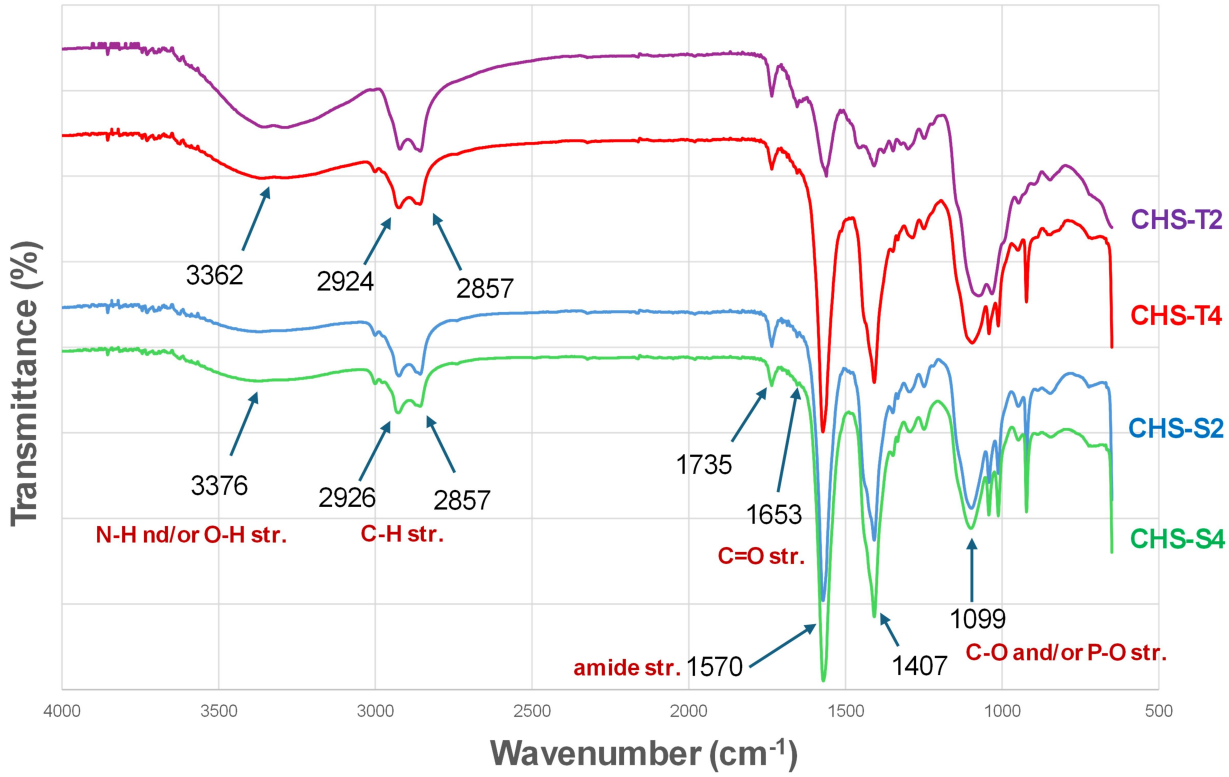

Figure 3. Infrared (IR) spectra of chitosan nanoparticle (CHS-NP) formulations crosslinked with 0.136 and 0.340 mmol polyphosphate [sodium tripolyphosphate (TPP) or sodium hexametaphosphate (SHMP)]/mg of CHS.

CUR release from CHS-based NPs

Figure 4 presents the cumulative permeation profiles of CUR through the membrane after loaded NPs and plain CUR solution were placed in the donor chamber. Naturally, free CUR in a plain solution permeated through the membrane relatively faster than the entrapped CUR in the CHS-NPs. Figure 5 shows that by plotting $ln\left[1 - \left(\frac{V_r + V_d}{V_r \cdot Q_{tot}}\right)Q_{out}(t)\right] \cdot \left[\frac{-V_d \cdot V_r}{S(V_r + V_d)}\right]$ against time (Equation 18), the permeability coefficient (P) of

the membrane for CUR was obtained from the slope (R^2 = 0.998). The mean value of P was 0.00640 ± 0.00052 cm/h.

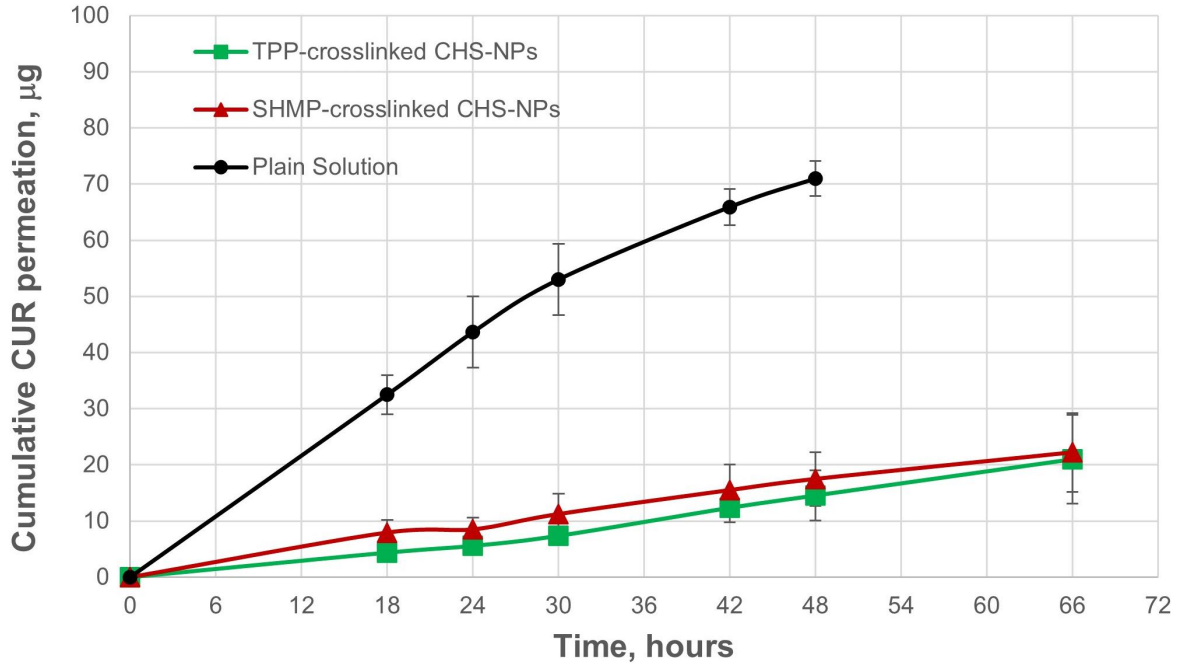

Figure 4. Curcumin (CUR) permeation (expressed as a cumulative quantity in the receiver chamber) through a polytetrafluoroethylene (PTFE) membrane. Free CUR in plain solution was compared with sodium tripolyphosphate (TPP)-crosslinked and sodium hexametaphosphate (SHMP)-crosslinked chitosan (CHS)-based nanoparticles (CHS-T1 and CHS-S1; 0.068 mmol polyanion/mg CHS). CHS-NPs: chitosan nanoparticles.

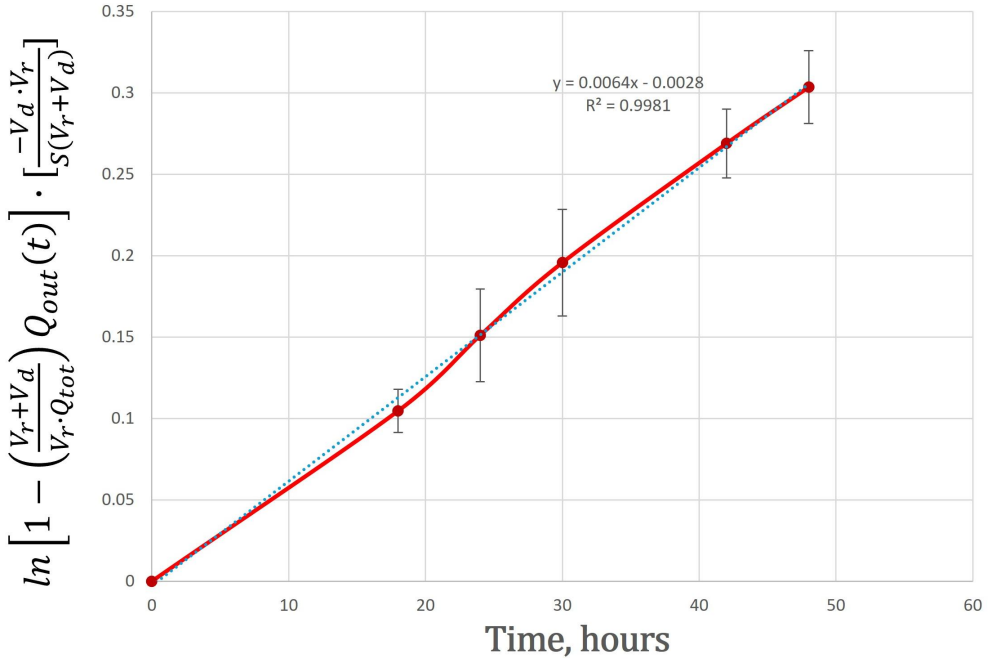

Figure 5. Determination of the permeability coefficient (*P*) of polytetrafluoroethylene (PTFE) membrane (0.1 µm pore size, 25 mm diameter) used in the release study of curcumin. P was derived from the slope of $ln\left[1-\left(\frac{V_r+V_d}{V_r\cdot Q_{tot}}\right)Q_{out}(t)\right]\cdot\left[\frac{-V_d\cdot V_r}{S(V_r+V_d)}\right]$ against t (according to Equation 18).

As shown in Figure 4, linear permeation rates of CUR were measured through the membrane after its release from TPP- and SHMP-crosslinked CHS-NPs. These linear permeation profiles are the result of the release rates of the entrapped CUR from the NPs, which limit and regulate the permeation fluxes of the free

molecules after their release. The release rates k_{rel} were derived from the plots of C_{out} versus $\frac{1}{(V_r + V_d)}\left[t - \frac{1}{a}(1 - e^{-at})\right]$, where the permeability coefficient (P) and the diffusion area S is comprised in function a (Equation 27). Figure 6 shows the method of calculating the k_{rel} of CUR from CHS-NP formulation prepared by ionic crosslinking with 0.068 mmol polyanion/mg CHS. The release rate of CUR from CHS-NPs crosslinked with 0.068 mmol TPP/mg CHS was 1.14 µg/h (CHS-T1) while at a higher TPP concentration of 0.340 mmol TPP/mg CHS (as in CHS-T4), the release rate was found to be similar (1.18 µg/h) (graph not shown).

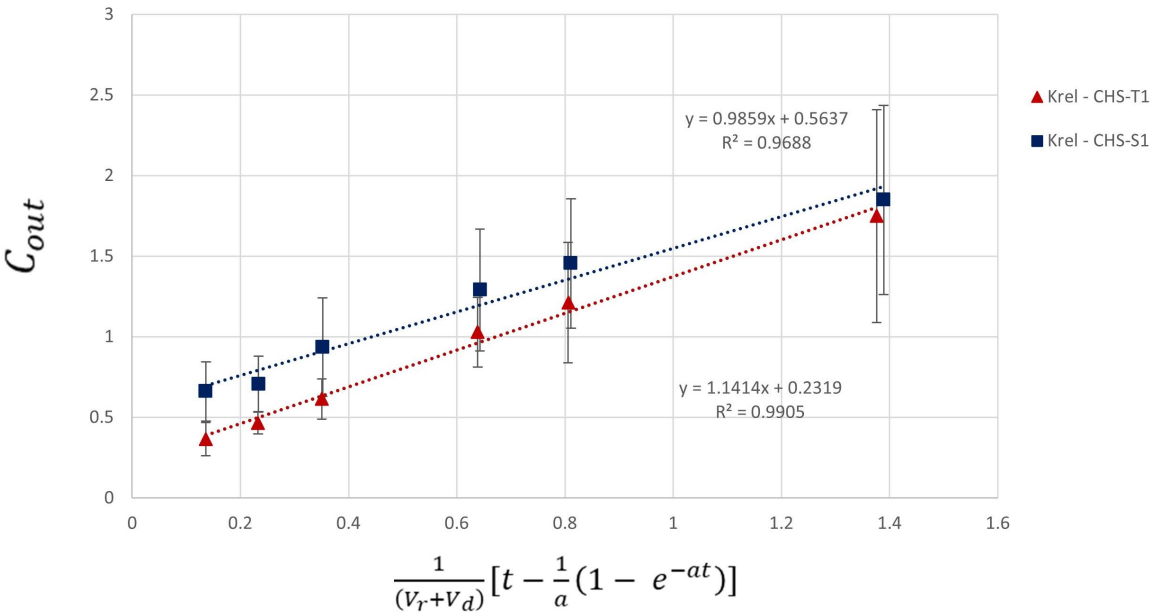

Figure 6. Calculation of the release rate constants of curcumin (CUR) k_{rel} from chitosan nanoparticles (CHS-NPs) according to Equation 27. CUR release constants were derived from the plots of C_{out} versus $\frac{1}{(V_r + V_d)}\left[t - \frac{1}{a}(1 - e^{-at})\right]$, and were determined as 1.1414 µg/h and 0.9859 µg/h for CHS-T1 and CHS-S1 (0.068 mmol polyanion/mg CHS), respectively.

Figure 7 demonstrates that SHMP levels in the range of 0.136–0.340 mmol/mg CHS resulted in 1.6–1.9-fold increase of the steady state permeation fluxes (0.57–0.66 µg/h) compared to 0.068 mmol SHMP/mg CHS (0.35 µg/h; Figure 4). More importantly, the calculated release rate constants (k_{rel}) (Figure 8), were about twice as high than the k_{rel} value of NPs with 0.068 mmol SHMP/mg CHS, that is, 1.86–2.10 µg/h for CHS-S2–S4 versus 0.98 µg/h for CHS-S1. A lag time of approximately 15 h prior to a steady state permeation flux of CUR appeared with CHS-S3 and CHS-S4 (0.226 mmol and 0.340 mmol SHMP/mg CHS), a significantly shorter lag time when CHS-S2 (0.136 mmol SHMP/mg CHS) was tested (Figure 7), and a total absence of a lag time when CHS-S1 (0.068 mmol SHMP/mg CHS) was tested (Figure 4).

Discussion

Characterization

The slight increase in the size of SHMP-crosslinked NPs compared to the TPP-crosslinked NPs (Table 2) was probably due to the larger SHMP molecules, which increased the space between CHS linear chains. TPP at a concentration of 0.340 mmol/mg CHS demonstrated a significant decrease in CUR loading and in the calculated EE. As this deviation had been repeatedly confirmed, it was postulated that at the high concentration of TPP, having a smaller molecular size (relative to SHMP), the NPs turned out to be denser and less permeable to CUR molecules. In addition, this finding may also be related to CUR's poor water solubility. When a water-soluble active agent is used, it usually dissolves in the CHS solution, then the crosslinker is added dropwise [21, 46]. Here, CUR was added concomitantly with the crosslinker, which

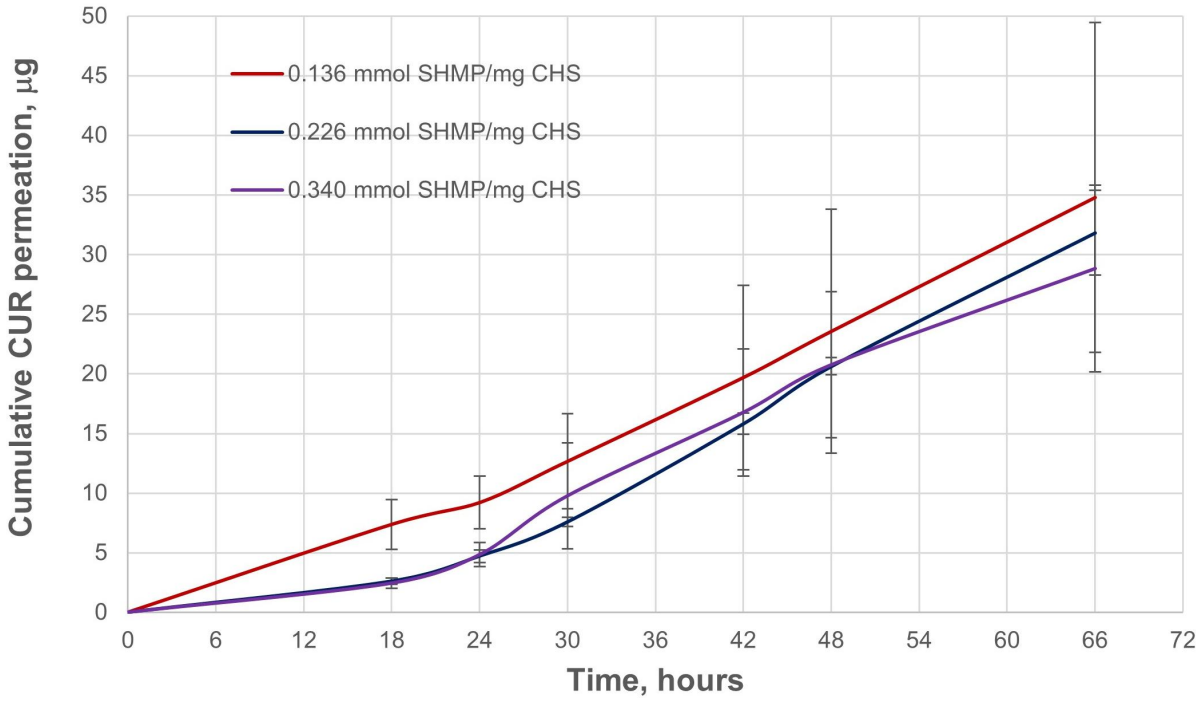

Figure 7. Curcumin (CUR) permeation (expressed as a cumulative quantity in the receiver chamber) through a polytetrafluoroethylene (PTFE) membrane. The permeation of free CUR molecules only through the membrane after they are released from sodium hexametaphosphate (SHMP)-crosslinked chitosan (CHS)-based nanoparticles (CHS-S2–S4; 0.136, 0.226, and 0.340 mmol polyanion/mg CHS).

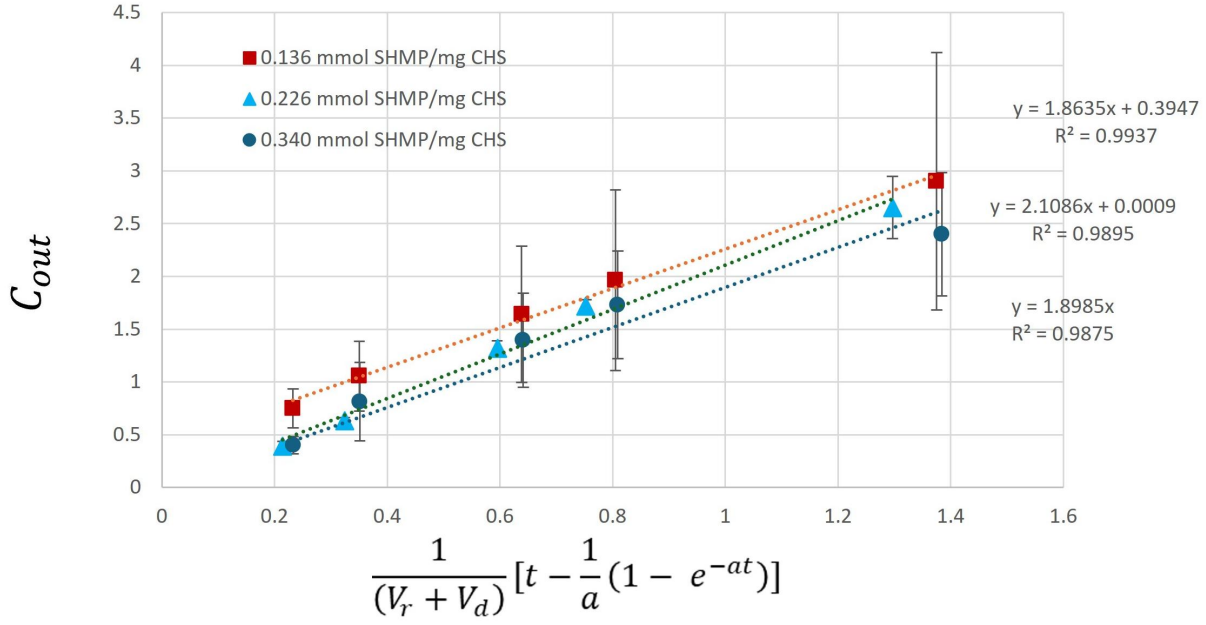

Figure 8. Calculation of the release rate constants of curcumin k_{rel} from chitosan nanoparticles (CHS-NPs) according to Equation 27. Curcumin release constants were derived from the plots of C_{out} versus $\frac{1}{(V_r + V_d)}\left[t - \frac{1}{a}(1 - e^{-at})\right]$, and were determined as 1.8635 µg/h, 2.1086 µg/h, and 1.8985 µg/h for CHS-S2, CHS-S3, and CHS-S4 [0.136 mmol, 0.226 mmol, and 0.340 mmol sodium hexametaphosphate (SHMP)/mg CHS], respectively.

may cause CUR to compete with TPP resulting in less available CUR during NPs' formation. Thus, at higher TPP concentrations, denser particles are formed faster, turning out to be less permeable to CUR.

As ζ potential is defined as the electrical potential at the interfacial surface of the particles, the decrease in the potential can be explained by the binding of the polyanion molecules on the surface of the unloaded CHS-NPs, thus neutralizing in part the positively charged surface. The increase in the potential noted in CUR-loaded CHS-NPs, can be explained therefore by the attraction of CUR molecules on the surface resulted

in protection of the surficial ammonium cations by preventing interaction with the polyanion. This mechanism preserves the original ζ potential of the non-crosslinked CHS. The difference between the two polyphosphate crosslinkers, which is expressed in NPs at the low concentration of 0.068 mmol polyanion/mg CHS, is probably due to the larger molecular structure of SHMP compared to the TPP molecule. At low concentration, SHMP molecules create NPs mostly by binding onto the outer amine groups rather than into their inner core. When higher SHMP concentrations are used, the crosslinking turns out to be more uniformly distributed during the NP formation, and the ionic bonds are evenly created along all the polymer chains.

FTIR analysis provided further insight into these structural differences. Two stretching peaks at 1,735 cm^{-1} and 1,407 cm^{-1} did not appear in CHS spectra or in the IR spectra related to pure polyphosphates. These stretching peaks, therefore, seem to be associated with acetate anion stretching and the ionic interactions of the positively charged amine groups on the CHS's backbones and the negatively charged acetate groups [47]. Bhumkar and Pokharkar [48] noted that in the FTIR spectra of TPP-crosslinked CHS (freeze-dried particles) the band of amide I at 1,655 cm^{-1} disappeared and two new peaks at 1,645 cm^{-1} and 1,554 cm^{-1} appeared, which they attributed to the linkage between the phosphoric and ammonium ions; however, such features were not observed in the present study. The higher intensity of C–H, N–H, and O–H vibrations observed in TPP-crosslinked NPs, particularly CHS-T2, likely reflects closer structural proximity between CHS chains, while reduced vibrational intensity at low TPP concentration is attributable to fewer ionic interactions.

CUR release

The release profiles of drugs and active agents entrapped in NPs in general and in CUR-loaded CHS-NPs in particular [43] have been usually determined using the conventional dialysis bag method [15, 49]. However, since any method involving a membrane is dependent on its permeability coefficient for the tested drug, a technique allowing improved precision of the permeability coefficient measurement may be advantageous over the commonly used dialysis tubing. The use of Franz diffusion cell system for evaluating drug release from NPs can provide adequate measures of the membrane's surface area as well as the volumes of the donor and the receiver solutions [35, 36].

As CUR release (and membrane permeation) from TPP-crosslinked CHS-NPs was not dependent on TPP concentrations in the given range, the effect of SHMP levels was also examined. The findings were quite different from TPP crosslinking, as the cumulative permeation profiles and the release rates of CUR were relatively higher.

This interesting finding complemented and supported our previous assessment (see above) that at low levels of SHMP, the crosslinking bonds concentrate mainly in the outer shell of the NPs, thus hindering and delaying the release of the entrapped CUR. At higher concentrations of SHMP, the crosslinking bonds are more uniformly distributed along the polymeric chains, enabling fluent diffusion of CUR outwards after a relatively short lag time. Naturally, a lag time appears as more crosslinking bonds are formed, which prolong the time to reach a steady state release rate. This aligns well with the ζ potential data (Table 2), where SHMP potential increased with concentration from 15.6 ± 1.6 mV to 34.6 ± 1.9 mV at SHMP levels of 0.068 mmol/mg up to 0.340 mmol/mg, respectively, suggesting a change in surface charge density. The other finding that CUR release profiles from TPP-crosslinked CHS-NPs did not have a notable lag time of the release can be explained by (a) the small molecular weight of TPP that formed relatively denser NPs and decreased the release rate of CUR, (b) the slow rate of the steady-state release of CUR resembled the rate of the initial release. The increased permeation and release rates of CUR from SHMP-crosslinked CHS-NPs, which are in contrast with the permeation and release of CUR from TPP-crosslinked CHS-NPs, are due to the high molecular weight and "bulky" structure of SHMP crosslinker. Although the repeating hexametaphosphate units provide more potential negatively charged phosphate sites than the linear triphosphate chain of TPP, it has been demonstrated that NPs formed by reaction with SHMP are larger than those fabricated with TPP. This finding confirms a previous report by Abdelgawad and Hudson [46], with similar NPs also prepared at pH = 5. A quantitative porosity characterization of the NPs was not

performed in the present study. It is therefore hypothesized and suggested that if SHMP crosslinks CHS in a way that creates less regular or heterogeneous crosslinking domains, the resultant network can have larger voids or internal free volume, opposite to TPP that possesses shorter anionic chain and can produce a more compact and uniform ionic bridges.

The zero-order release kinetics obtained in the present study are in agreement with Nair et al. [43], who also examined the release of CUR from CHS-based NPs. Using the dialysis bag method, this previous report showed that 41.5% of CUR were released from TPP-crosslinked CHS-NPs at pH = 5, and only about 19% were released at pH = 7.4 over a 24-hour period [43]. The data obtained in the present report demonstrated comparable results, in which less than 10% of CUR were permeated through the membrane at pH = 7.4 by 24 h and about 17% over 66 h period when TPP-crosslinked CHS-NPs were tested. However, since a membrane permeability is obviously a limiting factor, the calculated release rates of CUR from the CHS-NPs according to Equation 27, were between 1.1–1.2 μg/h, i.e., 22–24% of CUR were released by 24 h with the four TPP concentrations used. In contrast to TPP crosslinking, CHS-NPs crosslinked with SHMP at levels ranging between 0.136–0.340 mmol/mg CHS showed a higher release rates with notable lag times. A different study using CHS-NPs was reported by Gomathi et al. [50], who used direct dissolution testing to evaluate the release rates of 5-fluorouracil from NPs crosslinked by TPP and SHMP. The release patterns of the this drug from both types of NPs included an initial burst followed by a sustained release [50]. These different patterns stem from a highly water soluble drug adherent to the surface of the NPs followed by the release of the drug trapped within the core. The release from CHS-NPs is not only dependent on the drug properties, but on the NP properties as well. CHS-NP composition and mode of manufacturing, such as crosslinker type, CHS to crosslinker ratio, pH, temperature, and stirring speed are important factors that dictate the in-vitro and in-vivo release profiles of the active compound [48, 51, 52].

To conclude, in this study, TPP- and SHMP-crosslinked CHS-NPs were prepared with loaded CUR as a model active agent, characterized, and compared for their physical properties and in-vitro release of their loading. It was shown that although SHMP resulted in a slight increase in the mean particle size in comparison to the particle size of TPP crosslinker, the EE and CUR loading were constant at the various concentrations of this polyanion. TPP crosslinking, however, demonstrated a decrease in EE at a relatively high concentration of the agent, probably by narrowing the space between the polymeric chains. As indicated by ζ potential measurement, TPP crosslinking at all levels was more uniformly distributed inside the NPs whereas the larger molecular weight SHMP at a low concentration (0.068 mmol/mg CHS) creates NPs mostly by binding to the ammonium groups on the surface. As further described in this study, drug released from NPs can be more adequately determined by Franz diffusion cell system. The method which has been established and developed by our group is based on a model that the drug is first released from the NP into the medium inside the donor chamber and subsequently diffuses through the membrane into the receiver chamber. The release rate of the drug from the particles can be evaluated only if the permeability coefficient of the membrane (P) is determined. After calculating P, the release rates were derived. It has been found that the release rates of CUR from CHS-NPs crosslinked by SHMP at concentrations higher than 0.136 mmol/mg CHS were about twice as high than the release rates of CUR from TPP-crosslinked CHS-NPs, accompanied by notable lag times. This significant increase in the release rates of CUR from SHMP-crosslinked CHS-NPs is explained by the high molecular weight and the large structure of this crosslinker compared to the small tripolyphosphate molecules. To conclude, this report demonstrates the complexity of CHS-based nano systems. The results can be considered as one more step in the mechanistic understanding of CHS formulations, therefore, they are practically useful for any pharmaceutical scientist working in the field.

Abbreviations

CHS: chitosan

CHS-NPs: chitosan nanoparticles

CUR: curcumin

DDW: double-distilled water

DMSO: dimethyl sulfoxide

EE%: encapsulation (or entrapment) efficiency percentage

FTIR: Fourier transform infrared spectroscopy

HPLC: high-performance liquid chromatography

IR: infrared

NPs: nanoparticles

NTA: nanoparticle tracking analysis

PBS: phosphate buffered saline

PTFE: polytetrafluoroethylene

SHMP: sodium hexametaphosphate

TEM: transmission electron microscopy

TPP: sodium tripolyphosphate

ζ: zeta

Supplementary materials

The supplementary figure for this article is available at: https://www.explorationpub.com/uploads/Article/file/1008157_sup_1.pdf.

Declarations

Acknowledgments

The authors are grateful for the professional assistance and technical support of the staff at Ilze Katz Institute for Nanoscale Science & Technology.

Author contributions

IE: Investigation, Formal analysis, Visualization, Writing—original draft. DY: Investigation, Formal analysis, Writing—review & editing. SBS: Conceptualization, Writing—review & editing. ACS: Conceptualization, Supervision, Formal analysis, Visualization, Writing—original draft, Writing—review & editing. All authors read and approved the submitted version.

Conflicts of interest

Amnon C. Sintov, who is the Editorial Board Member of Exploration of Drug Science, had no involvement in the decision-making or review process of this manuscript. The other authors declare that they have no known competing financial interests or personal relationships that could have appeared to influence the work reported in this paper.

Ethical approval

Not applicable.

Consent to participate

Not applicable.

Consent to publication

Not applicable.

Availability of data and materials

The data that supports the findings of this study are available from the corresponding author upon reasonable request.

Funding

This research received funding from B.G. Negev (BGN) (the tech-transfer company of Ben-Gurion University of the Negev). The funder had no role in study design, data collection and analysis, decision to publish, or preparation of the manuscript.

Publisher's note

Open Exploration maintains a neutral stance on jurisdictional claims in published institutional affiliations and maps. All opinions expressed in this article are the personal views of the author(s) and do not represent the stance of the editorial team or the publisher.

References

1. das Neves J, Bahia MF, Amiji MM, Sarmento B. Mucoadhesive nanomedicines: characterization and modulation of mucoadhesion at the nanoscale. Expert Opin Drug Deliv. 2011;8:1085–104. [DOI] [PubMed]
2. Hasnain MS, Nayak AK. Chitosan as mucoadhesive polymer in drug delivery. In: Hasnain MS, Beg S, editors. Chitosan in Drug Delivery. Elsevier; 2022. pp. 225–46.
3. Ahmad K, Zhang Y, Chen P, Yang X, Hou H. Chitosan interaction with stomach mucin layer to enhances gastric retention and mucoadhesive properties. Carbohydr Polym. 2024;333:121926. [DOI] [PubMed]
4. Shariatinia Z. Pharmaceutical applications of chitosan. Adv Colloid Interface Sci. 2019;263:131–94. [DOI] [PubMed]
5. Panda PK, Sadeghi K, Park K, Seo J. Regeneration Approach to Enhance the Antimicrobial and Antioxidant Activities of Chitosan for Biomedical Applications. Polymers (Basel). 2022;15:132. [DOI] [PubMed] [PMC]
6. Zhang X, Liang Y, Huang S, Guo B. Chitosan-based self-healing hydrogel dressing for wound healing. Adv Colloid Interface Sci. 2024;332:103267. [DOI] [PubMed]
7. Jafernik K, Ładniak A, Blicharska E, Czarnek K, Ekiert H, Wiącek AE, et al. Chitosan-Based Nanoparticles as Effective Drug Delivery Systems-A review. Molecules. 2023;28:1963. [DOI] [PubMed] [PMC]
8. Jha R, Mayanovic RA. A Review of the Preparation, Characterization, and Applications of Chitosan Nanoparticles in Nanomedicine. Nanomaterials (Basel). 2023;13:1302. [DOI] [PubMed] [PMC]
9. Bashir SM, Ahmed Rather G, Patrício A, Haq Z, Sheikh AA, Shah MZUH, et al. Chitosan Nanoparticles: A Versatile Platform for Biomedical Applications. Materials (Basel). 2022;15:6521. [DOI] [PubMed] [PMC]
10. Luppi B, Bigucci F, Cerchiara T, Zecchi V. Chitosan-based hydrogels for nasal drug delivery: from inserts to nanoparticles. Expert Opin Drug Deliv. 2010;7:811–28. [DOI] [PubMed]
11. Elkomy MH, Ali AA, Eid HM. Chitosan on the surface of nanoparticles for enhanced drug delivery: A comprehensive review. J Control Release. 2022;351:923–40. [DOI] [PubMed]
12. Baek JS, Cho CW. Surface modification of solid lipid nanoparticles for oral delivery of curcumin: Improvement of bioavailability through enhanced cellular uptake, and lymphatic uptake. Eur J Pharm Biopharm. 2017;117:132–40. [DOI] [PubMed]

13. Grenha A. Chitosan nanoparticles: a survey of preparation methods. J Drug Target. 2012;20:291–300. [DOI] [PubMed]
14. Yanat M, Schroën K. Preparation methods and applications of chitosan nanoparticles; with an outlook toward reinforcement of biodegradable packaging. React Funct Polym. 2021;161:104849. [DOI]
15. Tian XX, Groves MJ. Formulation and biological activity of antineoplastic proteoglycans derived from Mycobacterium vaccae in chitosan nanoparticles. J Pharm Pharmacol. 1999;51:151–7. [DOI] [PubMed]
16. Zoe LH, David SR, Rajabalaya R. Chitosan nanoparticle toxicity: A comprehensive literature review of in vivo and in vitro assessments for medical applications. Toxicol Rep. 2023;11:83–106. [DOI] [PubMed] [PMC]
17. Aibani N, Rai R, Patel P, Cuddihy G, Wasan EK. Chitosan Nanoparticles at the Biological Interface: Implications for Drug Delivery. Pharmaceutics. 2021;13:1686. [DOI] [PubMed] [PMC]
18. Jhaveri J, Raichura Z, Khan T, Momin M, Omri A. Chitosan Nanoparticles-Insight into Properties, Functionalization and Applications in Drug Delivery and Theranostics. Molecules. 2021;26:272. [DOI] [PubMed] [PMC]
19. Sarmento B, Ribeiro A, Veiga F, Sampaio P, Neufeld R, Ferreira D. Alginate/chitosan nanoparticles are effective for oral insulin delivery. Pharm Res. 2007;24:2198–206. [DOI] [PubMed]
20. Calvo P, Remuñán-López C, Vila-Jato JL, Alonso MJ. Novel hydrophilic chitosan-polyethylene oxide nanoparticles as protein carriers. J Appl Polym Sci. 1997;63:125–32. [DOI]
21. Sang Z, Qian J, Han J, Deng X, Shen J, Li G, et al. Comparison of three water-soluble polyphosphate tripolyphosphate, phytic acid, and sodium hexametaphosphate as crosslinking agents in chitosan nanoparticle formulation. Carbohydr Polym. 2020;230:115577. [DOI] [PubMed]
22. Saeed RM, Dmour I, Taha MO. Stable Chitosan-Based Nanoparticles Using Polyphosphoric Acid or Hexametaphosphate for Tandem Ionotropic/Covalent Crosslinking and Subsequent Investigation as Novel Vehicles for Drug Delivery. Front Bioeng Biotechnol. 2020;8:4. [DOI] [PubMed] [PMC]
23. Thandapani G, P SP, P N S, Sukumaran A. Size optimization and in vitro biocompatibility studies of chitosan nanoparticles. Int J Biol Macromol. 2017;104:1794–806. [DOI] [PubMed]
24. Hu Q, Luo Y. Chitosan-based nanocarriers for encapsulation and delivery of curcumin: A review. Int J Biol Macromol. 2021;179:125–35. [DOI] [PubMed]
25. Yu Y, Shen Q, Lai Y, Park SY, Ou X, Lin D, et al. Anti-inflammatory Effects of Curcumin in Microglial Cells. Front Pharmacol. 2018;9:386. [DOI] [PubMed] [PMC]
26. Yu X, Chen L, Tang M, Yang Z, Fu A, Wang Z, et al. Revealing the Effects of Curcumin on SH-SY5Y Neuronal Cells: A Combined Study from Cellular Viability, Morphology, and Biomechanics. J Agric Food Chem. 2019;67:4273–9. [DOI] [PubMed]
27. Liu S, Liu J, He L, Liu L, Cheng B, Zhou F, et al. A Comprehensive Review on the Benefits and Problems of Curcumin with Respect to Human Health. Molecules. 2022;27:4400. [DOI] [PubMed] [PMC]
28. Quispe C, Herrera-Bravo J, Javed Z, Khan K, Raza S, Gulsunoglu-Konuskan Z, et al. Therapeutic Applications of Curcumin in Diabetes: A Review and Perspective. Biomed Res Int. 2022;2022: 1375892. [DOI] [PubMed] [PMC]
29. Patel SS, Acharya A, Ray RS, Agrawal R, Raghuwanshi R, Jain P. Cellular and molecular mechanisms of curcumin in prevention and treatment of disease. Crit Rev Food Sci Nutr. 2020;60:887–939. [DOI] [PubMed]
30. Xu H, Ma Q, Qiu C, Wang J, Jin Z, Hu Y. Encapsulation and controlled delivery of curcumin by self-assembled cyclodextrin succinate/chitosan nanoparticles. Food Hydrocolloids. 2024;157:110465. [DOI]
31. Mishra B, Yadav AS, Malhotra D, Mitra T, Sinsinwar S, Radharani NNV, et al. Chitosan Nanoparticle-Mediated Delivery of Curcumin Suppresses Tumor Growth in Breast Cancer. Nanomaterials (Basel). 2024;14:1294. [DOI] [PubMed] [PMC]

32. Diaz-Ramirez J, Basasoro S, Torresi S, Eceiza A, Retegi A, Gabilondo N. Bacterial cellulose/thiolated chitosan nanoparticles hybrid antimicrobial dressing for curcumin delivery. Int J Biol Macromol. 2025;289:138836. [DOI] [PubMed]
33. Rezagholizade-shirvan A, Masrournia M, Fathi Najafi M, Behmadi H. Synthesis and characterization of nanoparticles based on chitosan-biopolymers systems as nanocarrier agents for curcumin: study on pharmaceutical and environmental applications. Polym Bull. 2022;80:1495–517. [DOI]
34. Ray L, Pal MK, Ray RS. Synergism of co-delivered nanosized antioxidants displayed enhanced anticancer efficacy in human colon cancer cell lines. Bioact Mater. 2017;2:82–95. [DOI] [PubMed] [PMC]
35. Sintov AC, Enden G. New doxorubicin nanoparticles engineered from calcium-crosslinked carbomer and a microemulsion precursor. Drug Dev Ind Pharm. 2017;43:830–8. [DOI] [PubMed]
36. Sintov AC. Nanoparticulate System Based on Calcium-Crosslinked Carbomer Retards Percutaneous Drug Permeation: New Insight Into Skin Barrier Functions. Pharm Res. 2022;39:3331–43. [DOI] [PubMed]
37. Algharib SA, Dawood A, Zhou K, Chen D, Li C, Meng K, et al. Preparation of chitosan nanoparticles by ionotropic gelation technique: Effects of formulation parameters and *in vitro* characterization. J Mol Struct. 2022;1252:132129. [DOI]
38. Janes KA, Fresneau MP, Marazuela A, Fabra A, Alonso MJ. Chitosan nanoparticles as delivery systems for doxorubicin. J Control Release. 2001;73:255–67. [DOI] [PubMed]
39. Hoang NH, Le Thanh T, Sangpueak R, Treekoon J, Saengchan C, Thepbandit W, et al. Chitosan Nanoparticles-Based Ionic Gelation Method: A Promising Candidate for Plant Disease Management. Polymers (Basel). 2022;14:662. [DOI] [PubMed] [PMC]
40. Muzzarelli RA. Genipin-crosslinked chitosan hydrogels as biomedical and pharmaceutical aids. Carbohydr Polym. 2009;77:1–9. [DOI]
41. Divya K, Jisha MS. Chitosan nanoparticles preparation and applications. Environ Chem Lett. 2017;16:101–12. [DOI]
42. Ukwubile CA, Otalu O, Okoro RN, Paul S. Antibacterial and anticancer synergy of chitosan NPs loaded with *Curcuma longa* (turmeric) extract against *Helicobacter pylori*-associated AGS gastric cancer cells. J Res Complement Med. 2025;2:59–69. [DOI]
43. Nair RS, Morris A, Billa N, Leong CO. An Evaluation of Curcumin-Encapsulated Chitosan Nanoparticles for Transdermal Delivery. AAPS PharmSciTech. 2019;20:69. [DOI] [PubMed]
44. Asif HM, Zafar F, Ahmad K, Iqbal A, Shaheen G, Ansari KA, et al. Synthesis, characterization and evaluation of anti-arthritic and anti-inflammatory potential of curcumin loaded chitosan nanoparticles. Sci Rep. 2023;13:10274. [DOI] [PubMed] [PMC]
45. Gupta PK, Hung CT, Perrier DG. Quantitation of the release of doxorubicin from colloidal dosage forms using dynamic dialysis. J Pharm Sci. 1987;76:141–5. [DOI] [PubMed]
46. Abdelgawad AM, Hudson SM. Chitosan nanoparticles: Polyphosphates cross-linking and protein delivery properties. Int J Biol Macromol. 2019;136:133–42. [DOI] [PubMed]
47. Cervera MF, Heinämäki J, de la Paz N, López O, Maunu SL, Virtanen T, et al. Effects of spray drying on physicochemical properties of chitosan acid salts. AAPS PharmSciTech. 2011;12:637–49. [DOI] [PubMed] [PMC]
48. Bhumkar DR, Pokharkar VB. Studies on effect of pH on cross-linking of chitosan with sodium tripolyphosphate: a technical note. AAPS PharmSciTech. 2006;7:E50. [DOI] [PubMed] [PMC]
49. Herdiana Y, Wathoni N, Shamsuddin S, Muchtaridi M. Drug release study of the chitosan-based nanoparticles. Heliyon. 2021;8:e08674. [DOI] [PubMed] [PMC]
50. Gomathi T, Alam MM, Al-Sehemi AG, Sudha PN, Pazhanisamy P, Vijayakumar S. Evaluation of sustained release and cytotoxicity studies of 5-fluorouracil loaded chitosan nanoparticles using sodium tripolyphosphate/sodium hexametaphosphate. Biomass Conv Bioref. 2024;15:26653–73. [DOI]

51. Warsito MF, Agustiani F. A review on factors affecting chitosan nanoparticles formation. IOP Conf Ser Mater Sci Eng. 2021;1011:012027.
52. Rostami E. Progresses in targeted drug delivery systems using chitosan nanoparticles in cancer therapy: A mini-review. J Drug Deliv Sci Technol. 2020;58:101813. [DOI]